Volume 5 | Number 6 | June 2014 | Pages 2103–2590

Chemical Science

www.rsc.org/chemicalscience

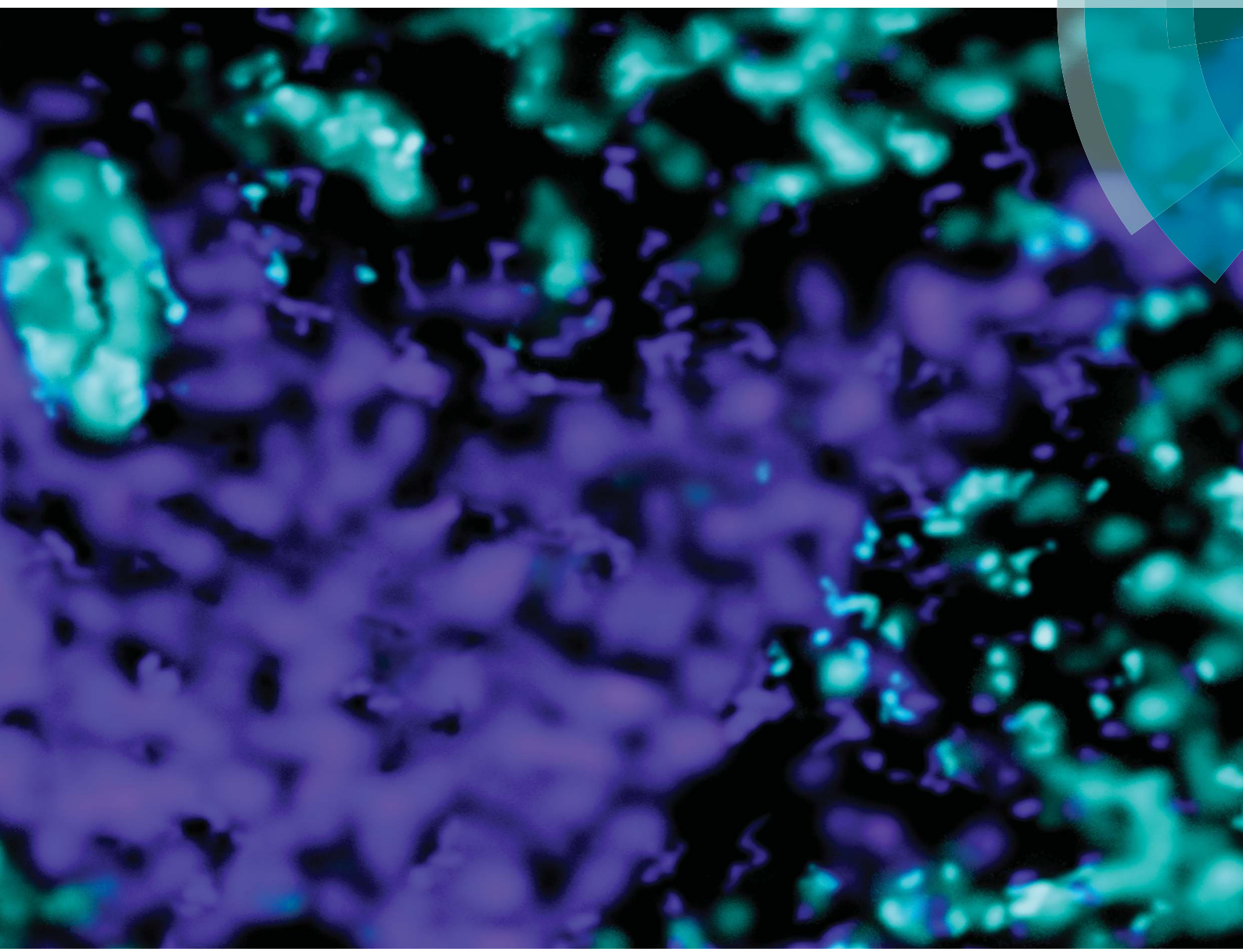

ISSN 2041-6520

ROYAL SOCIETY OF CHEMISTRY

EDGE ARTICLE

Philip A. Doble *et al.*

An iron–dopamine index predicts risk of parkinsonian neurodegeneration in the substantia nigra pars compacta

Chemical Science

EDGE ARTICLE

View Article Online
View Journal | View Issue

Cite this: *Chem. Sci.*, 2014, **5**, 2160

An iron–dopamine index predicts risk of parkinsonian neurodegeneration in the substantia nigra pars compacta†

Dominic J. Hare,[ab] Peng Lei,[b] Scott Ayton,[b] Blaine R. Roberts,[b] Rudolf Grimm,[c] Jessica L. George,[b] David P. Bishop,[a] Alison D. Beavis,[a] Sarah J. Donovan,[bd] Gawain McColl,[b] Irene Volitakis,[b] Colin L. Masters,[b] Paul A. Adlard,[b] Robert A. Cherny,[b] Ashley I. Bush,[b] David I. Finkelstein‡[b] and Philip A. Doble‡*[a]

The co-localization of iron and dopamine raises the risk of a potentially toxic reaction. Disturbance of the balance in this unique chemical environment makes neurons in the substantia nigra pars compacta (SNc) particularly vulnerable to parkinsonian neurodegeneration in the aging brain. In Parkinson's disease, these neurons degenerate coincident with an elevation in brain iron levels, yet relatively little is known about specific regional iron distribution with respect to dopamine. To directly appraise the iron–dopamine redox couple, we applied immuno-assisted laser ablation-inductively coupled plasma-mass spectrometry imaging to co-localize iron with the dopamine-producing enzyme tyrosine hydroxylase at the coronal level of the substantia nigra. We found that in the healthy brain the SNc does not contain the greatest concentration of iron within the midbrain, while the dopamine-rich environment in this region reflects an increased oxidative load. The product of iron and dopamine was significantly greater in the SNc than the adjacent ventral tegmental area, which is less susceptible to neuron loss in Parkinson's disease. Accordingly, this 'risk factor' was elevated further following 6-hydroxydopamine (6-OHDA) lesioning. Considering mounting evidence that brain iron increases with age, this measurable iron–dopamine index provides direct experimental evidence of a relationship between these two redox-active chemicals in degenerating dopaminergic neurons.

Received 17th December 2013
Accepted 24th January 2014

DOI: 10.1039/c3sc53461h

www.rsc.org/chemicalscience

Introduction

Degeneration of dopaminergic neurons in the substantia nigra coincident with a regional elevation in iron is a hallmark of Parkinson's disease (PD) pathology.[1] Numerous post-mortem studies have identified abnormalities in iron distribution throughout the basal ganglia, dating back to the original report by Lhermitte *et al.* in 1924.[2] Since then, iron has been associated with PD pathogenesis through a number of hypothesized mechanisms with the central tenet of iron-mediated production of reactive oxygen species.[3,4] One such proposed pathway implicates dopamine itself *via* iron-catalyzed degradation, which can produce either $OH^{\bullet}$ as a product of monoamine oxidase A and B activity, or reactive quinone species from autoxidation.[5,6] However, this route of neurotoxicity through dopamine oxidation does not reconcile with the progressive loss of nigrostriatal dopaminergic neurons that is accelerated in the substantia nigra pars compacta (SNc) region compared to adjacent dopamine-rich nuclei, such as the ventral tegmental area (VTA).[7]

Thus, we designed an imaging approach using laser ablation-inductively coupled plasma-mass spectrometry (LA-ICP-MS) to investigate the relationship between dopamine and iron in this vulnerable brain region. We took an immunohistochemical (IHC) metal-labeling technique to tag the rate-limiting enzyme in dopamine biosynthesis, tyrosine hydroxylase (TH), followed by the addition of a 10 nm gold nanoparticle-conjugated secondary antibody and subsequent silver enhancement; and combined it with LA-ICP-MS imaging (Fig. 1). Building on previous work,[8,9] we used this approach to visualize the distribution of both the IHC metal markers and cellular iron simultaneously in the same tissue section, allowing direct association of relative TH concentrations with fully quantitative iron levels at a high spatial resolution of up to 5 μm. As TH activity corresponds to catecholamine concentration and turnover,[10] we used it as a proxy for dopamine and were able to simultaneously examine iron and dopamine levels in both healthy mouse brains

[a]*Elemental Bio-imaging Facility, University of Technology, Broadway, Sydney, New South Wales, Australia. E-mail: philip.doble@uts.edu.au; Fax: +61 2 9514 1460; Tel: +61 2 9514 1792*

[b]*The Florey Institute of Neuroscience and Mental Health, The University of Melbourne, Parkville, Victoria, 3052, Australia*

[c]*Agilent Technologies, Santa Clara, California, 95051, United States of America*

[d]*Deakin University, Burwood, Victoria, 3125, Australia*

† Electronic supplementary information (ESI) available: Supplementary figures, tables and methods. See DOI: 10.1039/c3sc53461h

‡ These authors contributed equally.

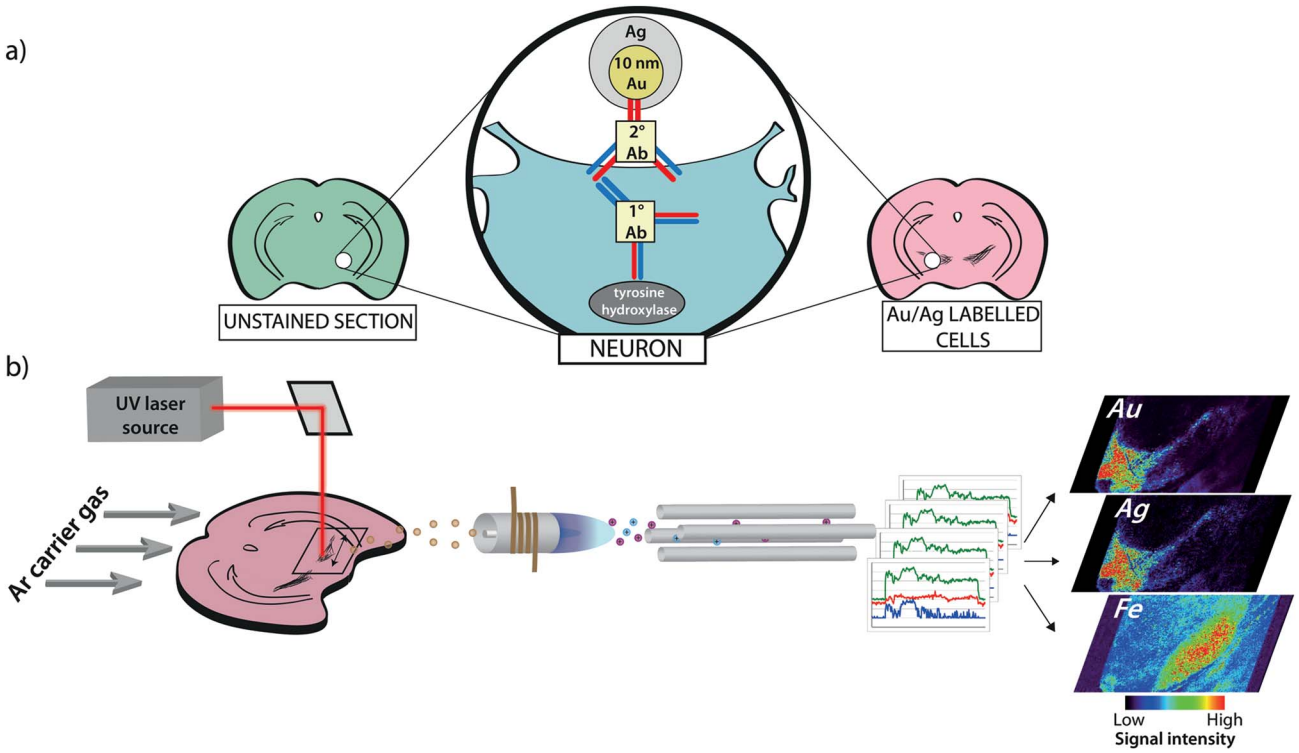

Fig. 1 Antigen labeling and imaging procedure. (a) 30 μm-thick coronal sections of brain tissue are immunolabeled with anti-TH followed by a secondary antibody conjugated to 10 nm gold (Au) nanoparticles. (b) Stained sections are imaged using a commercial LA-ICP-MS system. A 12 μm diameter UV ($\lambda = 193/213$ nm) laser beam is rastered across the sample surface, and the elemental content of ablated particles is detected in real time by atomic mass spectrometry. Data are reduced into spectral images where the Au and silver (Ag) response corresponds to immunolabeled TH-positive cells and is related to regional iron concentration.

and in the unilateral 6-hydroxydopamine (6-OHDA) lesion model of PD.

Results

Imaging of gold nanoparticle labeled TH-positive neurons

To demonstrate that our gold nanoparticle IHC approach was specific to TH-containing neurons, we stained brain sections ($n = 6$) using an anti-TH primary antibody, applied a pre-absorbed IgG secondary antibody conjugated to 10 nm gold nanoparticles enhanced with silver, and analysed the stained sections using our LA-ICP-MS bio-imaging procedure.[11] Images of gold, silver and iron were constructed with a spatial resolution equivalent to 12 μm (the total pixel area = 144 μm^2). Using serial sections for light microscopy, we correlated traditional IHC-stained sections with elemental images of gold nanoparticle-labeled cells at the level of the SN (anteroposterior from bregma −2.78 mm).[12] An anatomic reference plate was obtained from the open-access Allen Brain Atlas resource[13] (Fig. 2a). Histological features shown with 3,3′-diaminobenzidine (DAB) + Co + Ni-enhanced, neutral red (Nissl) counterstained sections (Fig. 2b), collected 30 μm posterior to LA-ICP-MS imaged sections were identified and interrelated with the Allen Brain Atlas reference plate and *in situ* hybridization (ISH) images of TH mRNA expression in the mesencephalon (Fig. 2c). To show correlation between gold images (Fig. 2d) and TH-positive, DAB-enhanced stained neurons in a serial section, we overlaid LA-ICP-MS images to show alignment between the gold signal response and the presence of dopaminergic neurons in the SNc and VTA (Fig. 2e). We observed that gold distribution throughout the midbrain region was consistent with TH-labeled cells identified by a traditional IHC technique. Gold deposition was confined primarily to the VTA and SNc, with a less intense signal response for gold in the SNr. Reduced gold signal intensity in the SNr compared to the SNc (39.5 ± 3.2 *vs.* 149 ± 15 counts per second; $p < 0.001$) was as a result of TH-containing dendrites from neurons in the SNc.[14] Conversely, a more intense gold signal indicative of a higher TH concentration was observed in the VTA when compared to the SNc (320 ± 28 counts per second; $p < 0.001$) (Fig. 2f). Silver enhancement was used to improve the image contrast for gold-labeled sections.[15,16] Correlation between gold and silver images was observed, though with elevated non-specific background silver staining arising from immersion of the sample in the silver enhancer solution (ESI Fig. 1†). Collectively, the consistent overlay between the gold signal and traditional TH-staining validated the protocol of IHC-LA-ICP-MS to visualize TH immunoreactivity, and so identify dopaminergic neurons.

Regional iron distribution in the midbrain

Spectral imaging, where multiple masses are monitored in a single LA-ICP-MS imaging experiment, allows direct spatial

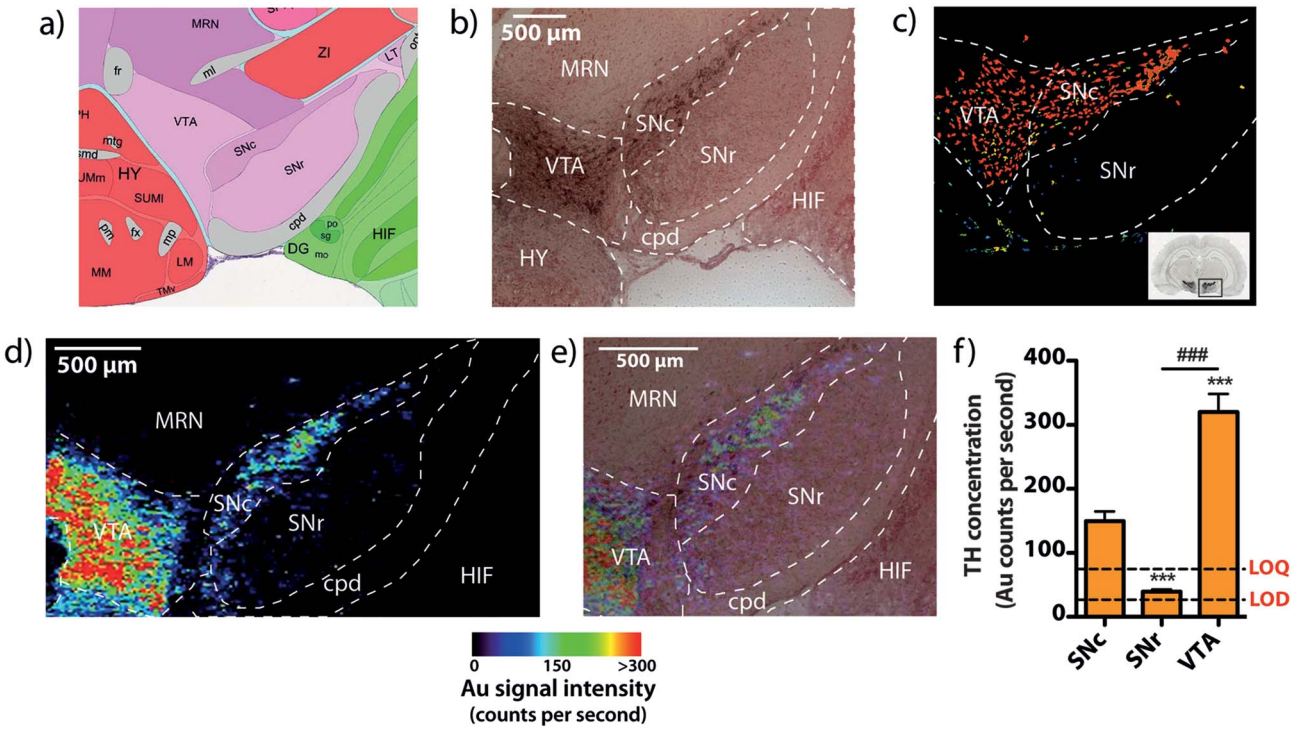

Fig. 2 Identifying TH-positive neurons *via* gold nanoparticle labeling. (a) A reference atlas plate obtained from the Allen Brain Atlas (Plate 81, bregma −2.78 mm) was used to identify (b) mesencephalic architecture in serial brain sections stained using traditional IHC, which was further correlated with (c) mRNA ISH images from the Allen Brain Atlas resource. (d) Imaging Au distribution demonstrates antigen-specific labeling of dopaminergic neurons in the substantia nigra pars compacta (SNc) and ventral tegmental area (VTA). (e) Overlaying the Au image with a micrograph from the serial IHC stained section correlates Au and TH-positive neuron localization. (f) Using Au signal intensity as a representative measure of TH, it was found that the highest concentration was present in the VTA, which contained approximately twice the mean amount of TH seen in the SNc (***/### $p < 0.001$). Abbreviations: cerebral peduncle (cpd), hippocampal formation (HIF), hypothalamus (HY), midbrain reticular nucleus (MRN), substantia nigra pars compacta (SNc), substantia nigra pars reticulata (SNr), ventral tegmental area (VTA), limit of detection (LOD), limit of quantification (LOD).

correlation between different metals. In addition to monitoring the masses of gold and silver, we also produced quantitative images of iron distribution in the mesencephalon to ascertain accurate regional iron concentrations in areas susceptible to neuron loss observed in PD. The collected data were used to construct three-dimensional contour plots depicting spatial metal distribution (Fig. 3a). This analysis revealed that iron content displayed compartmentalized distribution according to anatomical features at the granular layer of brain nuclei (Fig. 3b). The highest iron concentrations in this region did not correspond to TH-positive dopaminergic neurons in either the SNc or VTA regions; rather, the highest iron content in the midbrain was found in the SNr (Fig. 3c, ESI Fig. 2a†). We found that the SNc contained approximately 25% less iron than the adjacent SNr (SNr = 20.9 ± 0.7 µg g^{-1}, SNc = 14.4 ± 0.7 µg g^{-1}, $p < 0.001$). This was surprising, given the hypothesis that SNc neurons are vulnerable to PD neurodegeneration due to their relatively high basal iron levels, supporting the hypothesis that total iron levels alone within this nucleus may not be the risk factor in PD.[3] However, while the SNc contained less iron than the SNr, both regions displayed high iron levels compared to surrounding anatomical structures, suggesting that 'nigral' iron as a whole can be considered as a major repository within the midbrain (Fig. 3c).

We recently reported that around one quarter of brain iron is lost during the fixation and cryoprotection process,[17] though importantly, all brains used in this study underwent an identical sample preparation protocol. Additionally, Gałazka-Friedman *et al.*[18] noted that no significant change in deep brain iron content in the nigra occurs compared to fresh frozen tissue. To confirm this, the analytical validity of the quantitative data obtained by LA-ICP-MS imaging was evaluated by dissection and analysis of the iron content of the mesencephalon from the right hemisphere of the same mice, which was snap frozen at −80 °C immediately following brain removal. There was no significant difference between the total iron levels measured by traditional tissue dissection and solution nebulization ICP-MS and the mean mesencephalic iron concentration (combined SNc, SNr, VTA, midbrain reticular nucleus (MRN) and cerebral peduncle (CPD)) determined by LA-ICP-MS imaging (ICP-MS = 16.4 ± 1.3 µg g^{-1}, LA-ICP-MS = 15.4 ± 0.6 µg g^{-1}, $p = 0.532$, ESI Fig. 2b†). In addition to verifying that midbrain iron content is retained following fixation and cryoprotection, this further demonstrated the significant advantage of this technique over traditional dissection and digestion measurements; imaging by LA-ICP-MS retains detailed spatial information and analytical robustness that is otherwise lost by excision and analysis of the midbrain.

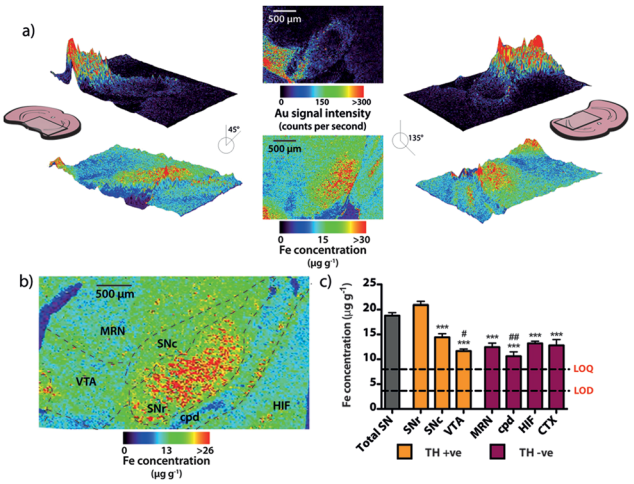

Fig. 3 Regional iron distribution in the mouse midbrain. (a) Three-dimensional contour images of Au and iron (Fe) distribution in the mesencephalon rotated 45 and 135 degrees from the normal. (b) Fe is distributed throughout the region (bregma −2.78) within granular nuclei, with (c) significantly more Fe present in the SNr than in the surrounding nuclei (ANOVA; *** $p < 0.001$ *vs.* SNr), including approximately 30% more Fe than in the adjacent SNc. There was also significantly less iron found in the VTA and cpd regions, relative to the SNc (ANOVA; # $p < 0.05$, ## $p < 0.01$; Games–Howell post-hoc test).

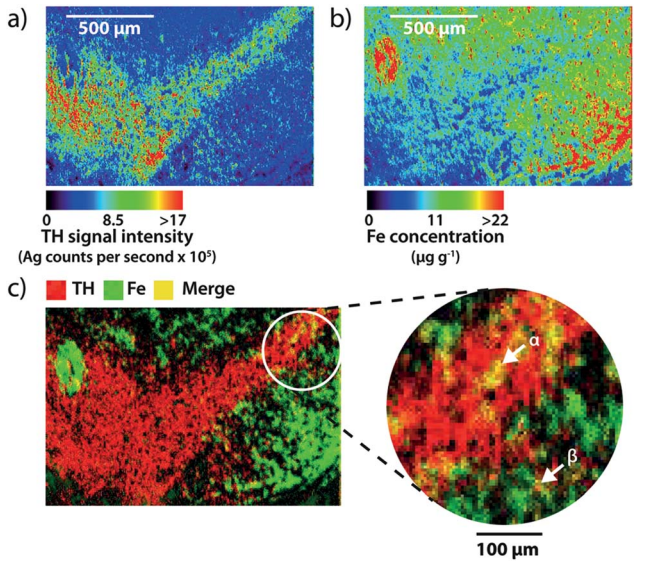

Fig. 4 Measuring iron content in dopaminergic neurons. (a) and (b) Spectral images of Ag and Fe distribution in TH-labeled sections for the quantification of neuronal iron content. (c) Merging both images identifies areas (yellow) where TH-positive regions (red) correlate with high Fe content (green). Cell bodies can be observed containing Fe in the SNc (α), with dendritic processes extending into the SNr (β).

High resolution imaging of iron in TH-positive neurons

Using spectral images obtained at a higher spatial resolution of 5 μm (pixel area = 25 μm^2) it is possible to quantify the amount of iron within individual cells (Fig. 4a and b). At this higher resolution, silver enhancement of gold nanoparticles was used to improve image quality. Gold particles serve as a point of nucleation for the autocatalytic reduction of metallic silver, increasing particle size,[19] and therefore LA-ICP-MS sensitivity. Mature TH-positive soma average 15–20 μm in diameter,[20] and thus, pixel coverage for a single dopaminergic cell body increased from 1 to at least 9 with the higher spatial resolution achieved *via* a 5 μm diameter laser beam. Merging silver and iron images (Fig. 4c) identified areas of TH and iron co-localization, corresponding to individual cell bodies in the SNc and dendritic processes projecting into the SNr.

Evidence for a relationship between dopamine and iron in the SNc and VTA

We used our gold-labeling and spectral imaging approach to study the iron and TH content of areas representing midbrain dopaminergic neurons. SNc dopaminergic neurons contain greater levels of iron compared to TH immunoreactive neurons in the VTA (14.1 ± 0.6 μg g^{-1} *vs.* 11.9 ± 0.5 μg g^{-1}, $p = 0.029$; ESI Fig. 3a†). In contrast, TH was more abundant in the VTA than in the adjacent SNc (SNc = 97.7 ± 13.9; VTA = 291 ± 33 gold counts per second, $p < 0.001$) (ESI Fig. 3b†). 99.1 ± 0.2% of the total VTA area imaged was TH positive, compared to 81.2 ± 3.2% for the SNc and 37.4 ± 6.7% for the SNr (ESI Fig. 3c†). The distribution of iron between TH-positive and -negative regions did not significantly differ (ESI Fig. 3d†). A small, yet significant negative correlation ($r_s = -0.199$, $p < 0.001$) was observed between iron and TH in all TH-positive pixels (ESI Fig. 3e†). This indicates that the contribution from the iron-dependent TH enzyme does not account for the majority of total iron. Instead, it is likely to be associated with the main iron-storage protein, ferritin.[21] We employed size exclusion chromatography (SEC) hyphenated to ICP-MS to examine the molecular weight species to which iron is bound in the soluble protein fraction within the mesencephalon (ESI Fig. 4†). We found that 84% of the total iron associated with soluble proteins in the midbrain was associated with the ferritin molecule.

A log-normalized plot of the distribution of iron in TH immunoreactive cells was remarkably similar in both the SNc and VTA (Fig. 5a). Both regions displayed a similar, relatively narrow range of iron concentrations per pixel (interquartile range of $\log_{10}$[Fe] : SNc = 0.148, VTA = 0.141, $n = 6$; Fig. 5b). To characterize the potential vulnerability imparted by high dopamine and iron co-localization within a defined area, we examined the product of dopamine and iron per μm (see the ESI experimental procedures†) in the SNc and VTA. We found that this dopamine–iron 'risk factor' was more than two-fold higher in the SNc (SNc = $13.6 \pm 2.0 \times 10^{-3}$ units μm^{-2}, VTA = $7.72 \pm 1.3 \times 10^{-3}$ units μm^{-2}, $p = 0.035$; Fig. 5c). This suggests that an upward shift in either dopamine or iron levels in this region could be responsible for the loss of dopaminergic neurons through elevated oxidative stress.

The dopamine–iron relationship is disturbed following 6-OHDA lesion

We used a unilateral 6-OHDA lesion of the SN to investigate if the relationship between dopamine and iron in the SNc is

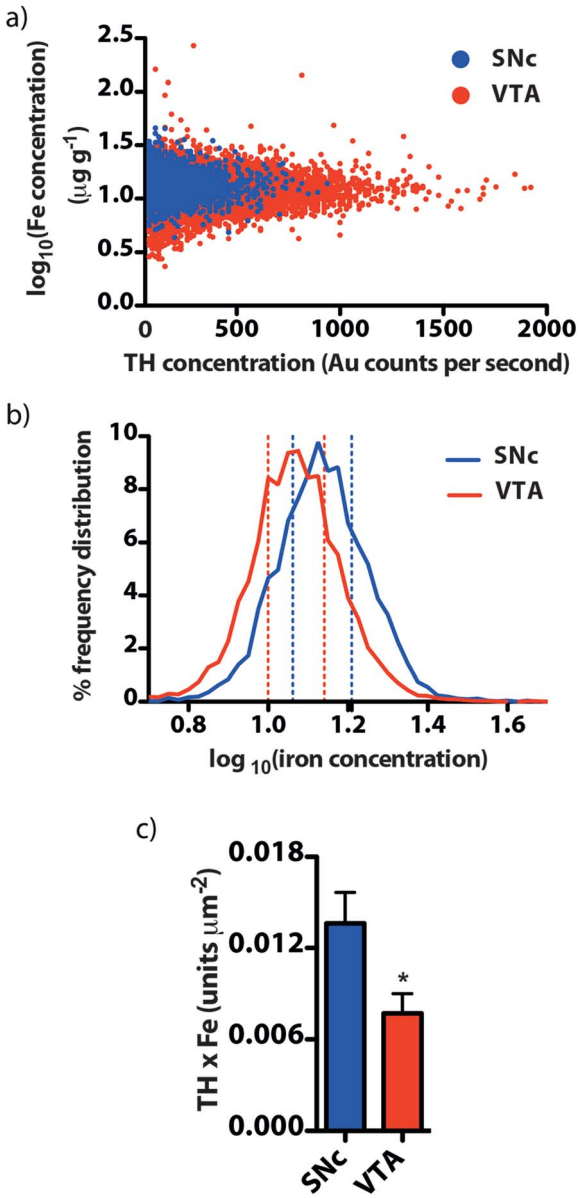

Fig. 5 Evidence for the oxidative vulnerability of the SNc. (a) A log plot of iron concentration against TH (and thereby, dopamine) showed a normal distribution in both the SNc and VTA. (b) The distribution of Fe within each region was remarkably similar, with the interquartile range (dashed lines) consistent between nuclei, though the mean Fe content of the SNc was greater. (c) The product of TH and Fe, corrected for the area of each region, was greatest in the vulnerable SNc, highlighting the enhanced potential for oxidative stress following an elevation in Fe levels, as has been observed in PD.

further perturbed in a parkinsonian model (Fig. 6a and b). Within the region of the SNc there was a noted increase in iron within TH-positive areas on the lesioned side (Fig. 6c). Mean TH intensity was decreased in the lesioned hemisphere, with a 20.5 ± 7.8% reduction and a non-significant downward trend ($p = 0.09$) in gold intensity in the lesioned SNc (Fig. 6d and e). Consistent with previous studies involving dopaminergic neurotoxins,[22] we observed a significant ipsilateral increase in iron concentration within surviving TH-positive areas in both the SNc (13.6 ± 1.4 *vs.* 11.6 ± 0.9 μg g^{-1}; $p < 0.05$) and the VTA (12.6 ± 0.4 *vs.* 10.9 ± 0.4 μg g^{-1}; $p < 0.01$) (Fig. 6f), suggesting that surviving cells were under some degree of stress following 6-OHDA exposure. We found that the product of dopamine and iron, already observed to be higher in the SNc than the adjacent VTA, was 42.5 ± 18.0% greater in the lesioned hemisphere compared to the contralateral midbrain (Fig. 6g), experimentally confirming our hypothesis that the product of dopamine and iron is a measurable index for parkinsonian neurodegeneration.

Discussion

Imaging metal species in biological tissue presents a complex analytical challenge: a suitable strategy requires a balance of sensitivity, selectivity and spatial resolution.[23] This work demonstrates how increased spatial resolution and our targeted gold-labeled IHC approach for LA-ICP-MS imaging is able to precisely visualize a protein of interest *in situ*, which can differentiate cell types based on unique chemical features and accurately quantify metals associated with them. Such data are usually obtained by non-quantitative histological techniques or by estimating the physical limits of an anatomical region for bulk metal assay, restricting the capacity for spatial measurements. Instead, imaging of cut tissue sections by LA-ICP-MS can quantify metals at micrometer spatial resolution without the need for excision and digestion, as has previously been required for iron assay in the midbrain region.[24] To date, previous examples of metal-tagged antibody labeling and LA-ICP-MS imaging have only described the distribution of a particular antigen, such as β-amyloid[8] and MUC-1 and HER2,[9] whereas we have demonstrated that simultaneous imaging of specific proteins and quantitative metal content is possible. Our data have also shown that a significant improvement in image resolution allows further differentiation of the iron content within subnuclei of the SN, providing a unique window into the mechanisms driving neuron death in PD.

We have thus used this approach to address a fundamental question in the field of PD research: what chemical environment makes neurons in the SNc particularly vulnerable to parkinsonian cytotoxicity? Healthy SNc dopaminergic neurons sustain high iron levels and are more susceptible to oxidation-dependent neurodegeneration.[4] Drugs targeting redox-active iron are effective in various animal models of PD,[24,25] and an increase in iron has been observed in the SN as a whole in PD subjects,[26] underlining the likely involvement of iron in PD pathogenesis. However, we have found that the direct appraisal of iron content in the SNc is obscured by its proximity with adjacent iron-rich nuclei, particularly the SNr, which contributes significant error when performing bulk analysis on the entire mesencephalon as an indicator of elevated SNc iron. Immunohistochemical approaches (*e.g.* Perls' and Turnbull's stains) to circumvent the problems with dissection are also limited by their sensitivity and have very limited quantitative capacity.

Consistent with human and rat studies using Perls' stain,[27,28] our results indicate that TH and high iron levels co-localize to the SNc and differentiate this region from surrounding nuclei.

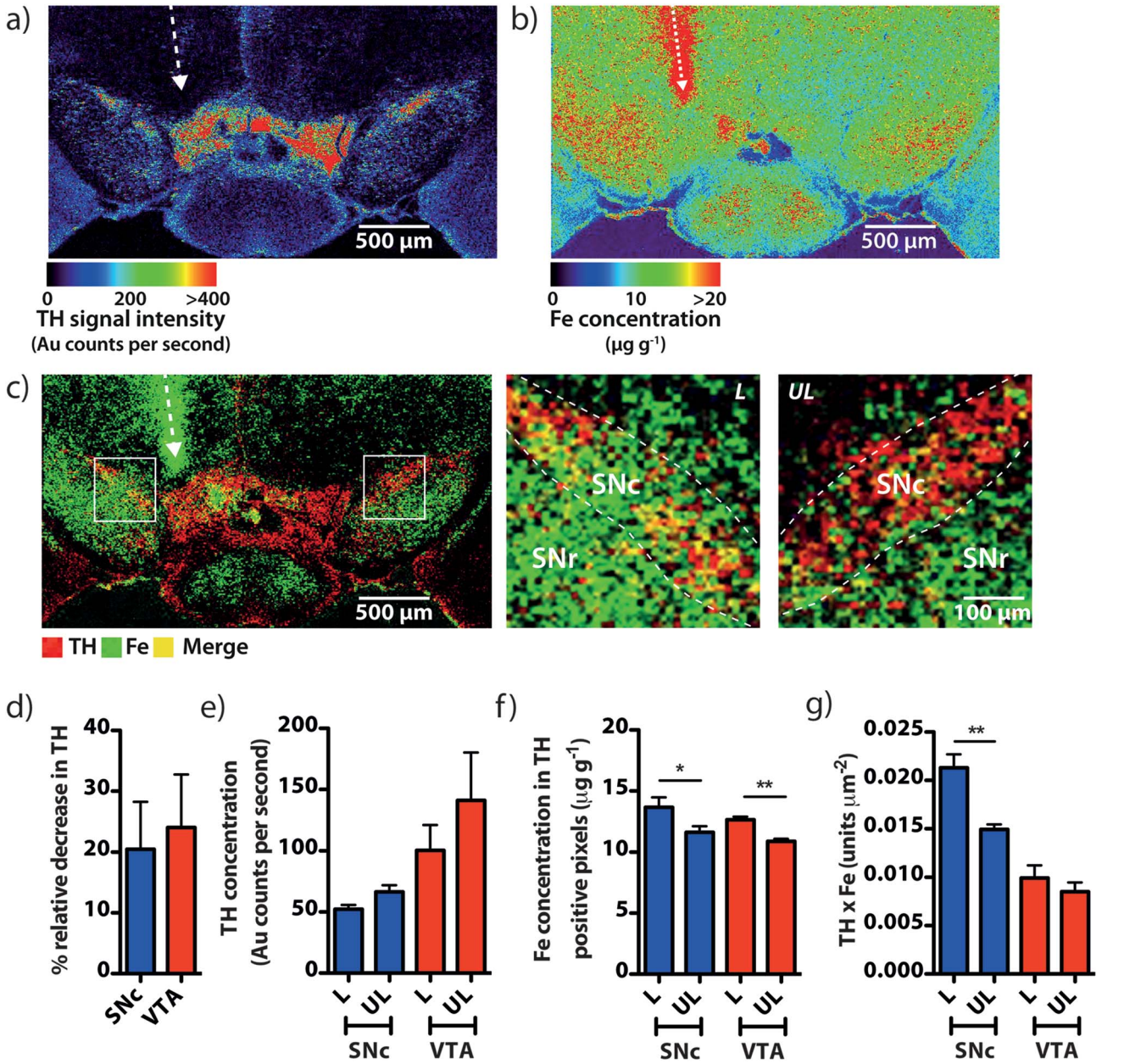

Fig. 6 The iron–dopamine index within the SNc is further elevated in a parkinsonian model. (a) and (b) TH and Fe images of a mouse midbrain 21 days after a stereotaxic 6-OHDA lesion. (c) Overlay of these two images reveals a marked increase in Fe and TH co-localization in the SNc in the lesioned hemisphere. (d) and (e) Unilateral 6-OHDA insult elicited a generalized decrease in TH intensity, coincident with (f) an increase in the Fe content of the surviving dopaminergic neurons. (g) The product of dopamine and Fe in the SNc was increased in comparison to the contralateral region.

The product of dopamine and iron is markedly higher in the SNc than in the adjacent VTA, which contains significantly higher TH levels, and the SNr, which contains relatively little TH or dopamine. We propose the singular occurrence of either higher basal iron (such as in the SNr) or higher TH/dopamine concentration (such as in the VTA) alone will not cause susceptibility to parkinsonian neurodegeneration. Vulnerability requires redox load from the combination of relatively high iron and dopamine together, as occurs in the SNc.[29] For the first time, this hypothesis is supported by our data showing that (i) the level of iron in the SNr is higher than in the SNc, though the SNr contains lower levels of dopamine; (ii) reciprocally, a high dopamine concentration is found in the VTA region, while this nucleus contains comparatively low iron; and (iii) only the SNc has both high iron and high dopamine levels. Within areas defined as TH immunoreactive, and therefore dopaminergic, our results indicate that the product of these two combustible components of dopamine oxidation mechanisms is most marked in the area of the brain known to suffer from cell loss in PD. This being the case, the redox load in the healthy brain would need to be countered by antioxidant defense. Indeed, when we accessed the Allen Brain Atlas[13] to view regional mRNA

expression of major antioxidant proteins, we found evidence of an increased capacity for reactive oxygen species scavenging by high expression of antioxidant proteins concentrated within the SNc. Localization of radical-scavenging enzymes including superoxide dismutase-1 (SOD1), Park7 and metallothionein-3 (MT3) all exhibit greater expression in the SNc compared to the VTA and SNr (ESI Fig. 6a–c†). SOD1 was recently shown to display increased activity in the substantia nigra of the PD brain,[30] and Park7 (also known as DJ-1) is an oxidative stress sensor, defects in which are associated with autosomal early-onset PD.[31] The metallothionein family, though not yet directly associated with idiopathic PD, is known to provide beneficial antioxidant activities[32] and a degree of protection against 6-OHDA insult in cell cultures.[33]

We used the *in vivo* 6-OHDA unilateral lesion model to show that disturbance of the already stressed oxidative load in the SNc can be measured using imaging LA-ICP-MS, and that this index may be reflective of the changing chemical environment within the Parkinson's disease brain. 6-OHDA-lesioned brains exhibit perturbations in iron levels within the basal ganglia,[34,35] a feature than can be arrested by administration of an iron chelator.[36,37] The decrease in TH was not confined to the SNc; a decrease was also observed in the VTA, consistent with other reports,[38] yet our measured product of dopamine and iron in the SNc was significantly higher in the lesioned hemisphere, compared to the contralateral region ($p < 0.01$).

In humans, the presence of neuromelanin in SNc dopaminergic neurons may further exacerbate vulnerability to oxidative damage. Neuromelanin displays a high affinity for iron,[39] and is present in comparatively small amounts in the rodent brain.[40,41] This additional store of iron in close proximity to high levels of dopamine has been suggested to precipitate heightened oxidative stress in idiopathic PD,[42,43] possibly by the release of redox-active iron following phagocytosis and degradation of iron-laden neuromelanin.[44] Indeed, the human VTA contains comparatively less neuromelanin than SNr neurons,[45] where neuromelanin synthesis is driven by excess intracellular catecholamine concentrations,[46] suggesting a possible upstream source of redox-active iron in the PD brain.

Our direct experimental evidence supports the proposed redox chemistry hypothesis in neurodegeneration involving dopamine and iron. The chemical mechanism by which dopamine and iron induce neurotoxicity involves the formation of an oxidized dopamine intermediary, aminochrome, a small amount of which is in turn reduced to the reactive leukoaminochrome-*o*-semiquinone radical. This mechanism, demonstrated in cultured hypothalamic cells in the presence of a quinone reductase inhibitor, requires labile iron(III).[47] A number of alternate mechanisms for the generation of reactive oxygen species from dopamine have been proposed, including production of 6-OHDA from fatty acid hydroperoxides,[48] 6,7-dihydroxytetrahydroisoquinoline[49] and anaerobic autoxidation;[50] all of which are mediated by iron(III). Our data suggest that the SNc, the area most vulnerable to iron-mediated neurodegeneration, exhibits a homeostatic relationship between these two reagents. Typically, iron in the cytoplasm of this metabolically active region is sequestered from dopamine in ferritin, or as part of a range of other iron-containing biomolecules. As iron levels in this region increase with age,[51] this delicate balance preventing a rise in labile iron is apt to be disrupted in PD; serum iron levels have recently been proposed as a possible marker for altered iron storage mechanisms[52] and a decrease in nigral ferritin is observed in the post-mortem PD brain,[53] which is in turn more heavily laden with iron.[26] The age-dependent rise in labile iron is likely to be proportional to the total iron content of each nucleus. As such, we also observed from the ISH image of mRNA expression that cytochrome b-561 (Cytb561), an integral membrane protein involved downstream of TH in the conversion of dopamine to norepinephrine by dopamine β-hydroxylase, is enriched in the SNc (ESI Fig. 6d†). Cytb561 is a known ferric reductase,[54] and dysfunction of this protein has been proposed as a possible source of labile iron in PD.[55,56]

Conclusions

Dopamine and iron produce a potentially hazardous chemical reaction when not sequestered from one another. In PD, it is hypothesized that iron dyshomeostasis disrupts chaperoning mechanisms that restrict iron interaction with dopamine, which leads to the generation of reactive oxygen species and neurotoxicity. We used a targeted imaging approach employing LA-ICP-MS to examine the distribution of both iron and the enzyme involved in dopamine biosynthesis in the rodent midbrain. We found that the region most vulnerable to parkinsonian neurodegeneration, the SNc, exhibited a measurable risk index of iron and dopamine; an index that was further elevated in the 6-OHDA-lesioned mouse brain. Our data provide key evidence that a direct association between iron and dopamine is involved in the mechanism of cell death in PD.

Methods and materials

Animals

All experiments were carried out in accordance with the local animal ethics committee requirements (Howard Florey Animal Ethics Committee) and National Health and Medical Research Council standards of animal care. 3-month-old male BL6/129sv mice ($n = 6$) were anaesthetized with sodium pentobarbitone (Lethabarb; 100 mg kg^{-1}) and perfused with 30 mL of 0.1 M phosphate buffered saline (PBS), pH 7.4. The brain was removed and placed in 4% (w/v) paraformaldehyde (Sigma-Aldrich) and 0.1 M PBS (4 °C), pH 7.4, overnight, then transferred to a sucrose solution (30% in PBS) for three days to cryoprotect the tissue. The brain was then rapidly frozen at −80 °C before sectioning through the substantia nigra (bregma −2.15 to −3.78 mm) at 30 μm intervals. Sections were mounted on standard soda glass microscope slides and stored at −80 °C until use.

For 6-OHDA lesions, mice ($n = 3$) were injected with 0.5 mg kg^{-1} atropine (Pharmacia) and 10 mg kg^{-1} xylazine (Troy Laboratories) prior to surgery. Mice were anaesthetized with 4% isofluorane (Forthane) in O_2 and maintained at 2% isoflurane for the duration of the surgery. A stereotaxic frame secured the head with a bite bar 3 mm above horizontal. Mice were injected with a chilled 1.65 mg mL^{-1} solution of 6-OHDA (Sigma) in

0.2 mg mL^{-1} ascorbic acid. A 26-gauge needle mounted to a syringe pump was inserted into the right median forebrain bundle (AP = 2.90 mm; ML = 1.1 mm; DV = 4.7 mm) through a hole drilled into the skull, through which 2 mL (3.3 mg) of 6-OHDA was slowly (0.5 μL min^{-1}) injected. Animals were killed 21 days after surgery and brains were recovered following the procedure used above.

Immunohistochemistry

After removal from storage, the sections were dried at room temperature and placed in a 4% paraformaldehyde solution for 1 minute. The sections were then rinsed in PBS 3 times and then incubated in a blocking solution of normal goat serum and Triton-X-100 in 0.1 M PBS. Following incubation, the sections were rinsed 3 times in PBS and then incubated overnight at room temperature with 1 : 3000 polyclonal anti-tyrosine hydroxylase (Millipore). Following overnight incubation, the sections were rinsed 3 times in PBS and incubated for 3 hours with the secondary antibody (goat anti-rabbit IgG (Poly-HRP)), 50 : 50 in 3% Triton-X-100 and 0.1 M PBS. Sections were then incubated for 30 minutes in 3,3′-diaminobenzidine (DAB) solution.[25] Sections were finally rinsed 3 times with PBS, counterstained with neutral red, cover slipped and photographed. Parallel sections (30 μm separation) were prepared for LA-ICP-MS analysis where the secondary antibody was substituted with goat anti-rabbit IgG preabsorbed with 10 nm gold nanoparticles (Abcam). Following a 3-hour incubation, the excess antibody was removed and sections were washed in 3 changes of PBS, after which sections were incubated for 30 minutes with a silver enhancement kit (BBI International). Excess silver solution was removed and sections were rinsed in 5 changes of deionized water. Sections were dried in a desiccator at room temperature for 24 hours and photographed. Sections were stored in an airtight container prior to analysis.

LA-ICP-MS imaging

Sections imaged at a 12 μm spatial resolution (total area = 144 μm^2 per pixel) were ablated using a New Wave Research UP213 laser ablation unit (Kenelec Scientific) fitted with a 25 × 25 cm large format cell. The laser unit was hyphenated to an Agilent 7500ce ICP-MS instrument fitted with a 'cs' lens assembly for enhanced sensitivity. Hydrogen (3 mL min^{-1}) was used as a reaction gas to remove $^{40}Ar^{16}O^{+}$ polyatomic interference on ^{56}Fe.[11] The system was tuned for sensitivity and minimal oxide formation ($^{232}Th^{16}O^{+}/^{232}Th < 0.3\%$) prior to analysis using NIST 612 (Trace Elements in Glass). The laser source was a Nd:YAG emitting a 213 nm laser beam in the fifth harmonic. A low energy fluence (0.3 J cm^{-2}) and high repetition rate (20 Hz) ensured adequate ablation of soft tissue without background contamination from the supporting glass matrix. For 5 μm (total area = 25 μm^2 per pixel) images, a New Wave Research NWR193 excimer laser unit (Kenelec Scientific) and an Agilent 7700s ICP-MS instrument were used with the same experimental conditions. Quantitative data were obtained by representative ablation of matrix-matched tissue standards using the method previously described.[57,58] Images were produced using in-house developed software (ISIDAS), ENVI 4.0 (Exelis Visual Information Solutions) and MayaVi2 (Enthought). Composite overlaid images were produced using ImageJ (NIH).

Solution ICP-MS analysis

See ESI Methods.†

Quantification of iron by LA-ICP-MS imaging

See ESI.†

SEC-ICP-MS analysis

See ESI.†

Statistics

See ESI.†

Acknowledgements

This work was supported by funds from the Australian Research Council, Agilent Technologies and Kenelec Scientific (as part of the Linkage Projects program, LP100200254), the Australian National Health & Medical Research Council, the Cooperative Research Centre for Mental Health, the Alzheimer's Association and Operational Infrastructure Support from the Victorian State Government. Software was developed by Dr Michael Lake of the Computational Research Support Unit of the University of Technology, Sydney. Dr Christine Austin assisted with manuscript editing. We would like to thank Jonas Marnell of Ethix Design for assistance with digital artwork.

Notes and references

1 T. Moos and E. Morgan, *Ann. N. Y. Acad. Sci.*, 2004, **1012**, 14–26.
2 J. Lhermitte, W. M. Kraus and D. McAlpine, *J. Neurol., Neurosurg. Psychiatry*, 1924, **5**, 195–208.
3 D. Berg, M. Gerlach, M. B. H. Youdim, K. L. Double, L. Zecca, P. Riederer and G. Becker, *J. Neurochem.*, 2001, **79**, 225–236.
4 L. Zecca, M. B. H. Youdim, P. Riederer, J. R. Connor and R. R. Crichton, *Nat. Rev. Neurosci.*, 2004, **5**, 863–873.
5 A. Hald and J. Lotharius, *Exp. Neurol.*, 2005, **193**, 279–290.
6 W. Linert, E. Herlinger, R. F. Jameson, E. Kienzl, K. Jellinger and M. B. H. Youdim, *Biochim. Biophys. Acta, Mol. Basis Dis.*, 1996, **1316**, 160–168.
7 N. Kubis, B. A. Faucheux, G. Ransmayr, P. Damier, C. Duyckaerts, D. Henin, B. Forette, Y. Le Charpentier, J. J. Hauw, Y. Agid and E. C. Hirsch, *Brain*, 2000, **123**, 366–373.
8 R. W. Hutchinson, A. G. Cox, C. W. McLeod, P. S. Marshall, A. Harper, E. L. Dawson and D. R. Howlett, *Anal. Biochem.*, 2005, **346**, 225–233.
9 J. Seuma, J. Bunch, A. Cox, C. McLeod, J. Bell and C. Murray, *Proteomics*, 2008, **8**, 3775–3784.
10 N. G. Bacopoulos and R. K. Bhatnagar, *J. Neurochem.*, 1977, **29**, 639–643.

11 J. Lear, D. J. Hare, F. Fryer, P. A. Adlard, D. I. Finkelstein and P. A. Doble, *Anal. Chem.*, 2012, **84**, 6707–6714.
12 K. B. J. Franklin and G. Paxinos, *The Mouse Brain in Stereotaxic Coordinates*, Academic Press, San Diego, 1997.
13 E. S. Lein, M. J. Hawrylycz, N. Ao, M. Ayres, A. Bensinger, A. Bernard, A. F. Boe, M. S. Boguski, K. S. Brockway and E. J. Byrnes, *Nature*, 2006, **445**, 168–176.
14 M. Wassef, A. Berod and C. Sotelo, *Neuroscience*, 1981, **6**, 2125–2139.
15 S. Eustis and M. A. El-Sayed, *Chem. Soc. Rev.*, 2006, **35**, 209–217.
16 P. Baptista, E. Pereira, P. Eaton, G. Doria, A. Miranda, I. Gomes, P. Quaresma and R. Franco, *Anal. Bioanal. Chem.*, 2008, **391**, 943–950.
17 D. J. Hare, J. L. George, L. Bray, I. Volitakis, A. Vais, T. M. Ryan, R. A. Cherny, A. I. Bush, C. L. Masters, P. A. Adlard, P. A. Doble and D. I. Finkelstein, *J. Anal. At. Spectrom.*, 2014, **29**, 565–570.
18 J. Gałazka-Friedman, E. R. Bauminger, A. Friedman, M. Barcikowska, D. Hechel and I. Nowik, *Movement Disord.*, 1996, **11**, 8–16.
19 S. Gupta, S. Huda, P. K. Kilpatrick and O. D. Velev, *Anal. Chem.*, 2007, **79**, 3810–3820.
20 O. Arias-Carrión, E. Yamada, N. Freundlied, M. Djufri, L. Maurer, G. Hermanns, B. Ipach, W.-H. Chiu, C. Steiner, W. H. Oertel and G. U. Höglinger, in *Birth, Life and Death of Dopaminergic Neurons in the Substantia Nigra*, ed. G. Giovanni, V. Di Matteo and E. Esposito, Springer, New York, 2009.
21 D. Kaur, S. Rajagopalan and J. K. Andersen, *Brain Res.*, 2009, **1297**, 17–22.
22 A. Schober, *Cell Tissue Res.*, 2004, **318**, 215–224.
23 R. McRae, P. Bagchi, S. Sumalekshmy and C. J. Fahrni, *Chem. Rev.*, 2009, **109**, 4780–4827.
24 D. Kaur, F. Yantiri, S. Rajagopalan, J. Kumar, J. Q. Mo, R. Boonplueang, V. Viswanath, R. Jacobs, L. Yang, M. F. Beal, D. DiMonte, I. Volitakis, L. Ellerby, R. A. Cherny, A. I. Bush and J. K. Andersen, *Neuron*, 2003, **37**, 899–909.
25 P. Lei, S. Ayton, D. I. Finkelstein, L. Spoerri, G. D. Ciccotosto, D. K. Wright, B. X. W. Wong, P. A. Adlard, R. A. Cherny, L. Q. Lam, B. R. Roberts, I. Volitakis, G. F. Egan, C. A. McLean, R. Cappai, J. A. Duce and A. I. Bush, *Nat. Med.*, 2012, **18**, 291–295.
26 P. D. Griffiths, B. R. Dobson, G. R. Jones and D. T. Clarke, *Brain*, 1999, **122**, 667–673.
27 P. Riederer, A. Dirr, M. Goetz, E. Sofic, K. Jellinger and M. Youdimt, *Ann. Neurol.*, 1992, **32**, S101–S104.
28 J. M. Hill and R. C. Switzer, *Neuroscience*, 1984, **11**, 595–603.
29 R. Ortega, P. Cloetens, G. Devès, A. Carmona and S. Bohic, *PLoS One*, 2007, **2**, e925.
30 K. M. Davies, S. Bohic, A. Carmona, R. Ortega, V. Cottam, D. J. Hare, J. P. M. Finberg, S. Reyes, G. M. Halliday, J. F. B. Mercer and K. L. Double, *Neurobiol. Aging*, 2014, **35**, 858–866.
31 V. Bonifati, P. Rizzu, M. J. van Baren, O. Schaap, G. J. Breedveld, E. Krieger, M. C. J. Dekker, F. Squitieri, P. Ibanez, M. Joosse, J. W. van Dongen, N. Vanacore, J. C. van Swieten, A. Brice, G. Meco, C. M. van Duijn, B. A. Oostra and P. Heutink, *Science*, 2002, **299**, 256–259.
32 H. J. You, D.-H. Oh, C. Y. Choi, D. G. Lee, K.-S. Hahm, A. R. Moon and H. G. Jeong, *Biochim. Biophys. Acta, Gen. Subj.*, 2002, **1573**, 33–38.
33 Y. P. Hwang, H. G. Kim, E. H. Han and H. G. Jeong, *Toxicol. Appl. Pharmacol.*, 2008, **231**, 318–327.
34 D. Blum, S. Torch, N. Lambeng, M. F. Nissou, A. L. Benabid, R. Sadoul and J. M. Verna, *Prog. Neurobiol.*, 2001, **65**, 135–172.
35 D. J. Hare, P. A. Adlard, P. A. Doble and D. I. Finkelstein, *Metallomics*, 2013, **5**, 91–109.
36 D. Ben-Shachar, G. Eshel, J. P. M. Finberg and M. B. Youdim, *J. Neurochem.*, 1991, **56**, 1441–1444.
37 D. Ben-Shachar, N. Kahana, V. Kampel, A. Warshawsky and M. B. H. Youdim, *Neuropharmacology*, 2004, **46**, 254–263.
38 R. Iancu, P. Mohapel, P. Brundin and G. Paul, *Behav. Brain Res.*, 2005, **162**, 1–10.
39 L. Zecca, R. Pietra, C. Goj, C. Mecacci, D. Radice and E. Sabbioni, *J. Neurochem.*, 1994, **62**, 1097–1101.
40 M. DeMattei, A. C. Levi and R. G. Fariello, *Neurosci. Lett.*, 1986, **72**, 37–42.
41 S. T. Kim, J. H. Choi, D. Kim and O. Hwang, *Neurosci. Lett.*, 2006, **396**, 263–268.
42 B. A. Faucheux, M. E. Martin, C. Beaumont, J. J. Hauw, Y. Agid and E. C. Hirsch, *J. Neurochem.*, 2003, **86**, 1142–1148.
43 K. Jellinger, E. Kienzl, G. Rumpelmair, P. Riederer, H. Stachelberger, D. Ben-Shachar and M. B. Youdim, *J. Neurochem.*, 1992, **59**, 1168–1171.
44 L. Zecca, L. Casella, A. Albertini, C. Bellei, F. A. Zucca, M. Engelen, A. Zadlo, G. Szewczyk, M. Zareba and T. Sarna, *J. Neurochem.*, 2008, **106**, 1866–1875.
45 C.-L. Liang, O. Nelson, U. Yazdani, P. Pasbakhsh and D. C. German, *J. Comp. Neurol.*, 2004, **473**, 97–106.
46 D. Sulzer, J. Bogulavsky, K. E. Larsen, G. Behr, E. Karatekin, M. H. Kleinman, N. Turro, D. Krantz, R. H. Edwards, L. A. Greene and L. Zecca, *Proc. Natl. Acad. Sci. U. S. A.*, 2000, **97**, 11869–11874.
47 I. Paris, P. Martinez-Alvarado, S. Cardenas, C. Perez-Pastene, R. Graumann, P. Fuentes, C. Olea-Azar, P. Caviedes and J. Segura-Aguilar, *Chem. Res. Toxicol.*, 2005, **18**, 415–419.
48 A. Pezzella, M. d'Ischia, A. Napolitano, G. Misuraca and G. Prota, *J. Med. Chem.*, 1997, **40**, 2211–2216.
49 A. Napolitano, A. Pezzella and G. Prota, *Chem. Res. Toxicol.*, 1999, **12**, 1090–1097.
50 U. El-Ayaan, E. Herlinger, R. F. Jameson and W. Linert, *J. Chem. Soc., Dalton Trans.*, 1997, 2813–2818.
51 L. Zecca, A. Stroppolo, A. Gatti, D. Tampellini, M. Toscani, M. Gallorini, G. Giaveri, P. Arosio, P. Santambrogio and R. G. Fariello, *Proc. Natl. Acad. Sci. U. S. A.*, 2004, **101**, 9843.
52 I. Pichler, F. Del Greco, M. Gögele, C. M. Lill, L. Bertram, C. B. Do, N. Eriksson, T. Foroud, R. H. Myers, PD GWAS Consortium, M. Nalls, M. F. Keller, International Parkinson's Disease Genomics Consortium, Wellcome Trust Case Control Consortium 2, B. Benyamin, J. B. Whitfield, Genetics of Iron Status Consortium, P. P.

Pramstaller, A. A. Hicks, J. R. Thompson and C. Minelli, *PLoS Med.*, 2013, **10**, e1001462.
53 D. T. Dexter, A. Carayon, F. Javoy-Agid, Y. Agid, F. R. Wells, S. E. Daniel, A. J. Lees, P. Jenner and C. D. Marsden, *Brain*, 1991, **114**, 1953–1975.
54 S. L. Rhodes and B. Ritz, *Neurobiol. Dis.*, 2008, **32**, 183–195.
55 C. P. Ponting, *Hum. Mol. Genet.*, 2001, **10**, 1853–1858.
56 Y. Ke and Z. Ming Qian, *Lancet Neurol.*, 2003, **2**, 246–253.
57 D. Hare, B. Reedy, R. Grimm, S. Wilkins, I. Volitakis, J. George, R. A. Cherny, A. I. Bush, D. I. Finkelstein and P. Doble, *Metallomics*, 2009, **1**, 53–58.
58 D. J. Hare, J. K. Lee, A. D. Beavis, A. van Gramberg, J. George, P. A. Adlard, D. I. Finkelstein and P. A. Doble, *Anal. Chem.*, 2012, **84**, 3990–3997.